ADVANCED ELECTRONIC MATERIALS
www.advelectronicmat.de

Spin- and Stress-Depending Electrical Transport in Nanoparticle Supercrystals: Sensing Elastic Properties of Organic Tunnel Barriers via Tunneling Magnetoresistance

Axel Dreyer, Thomas Rempel, Martin Gottschalk, Robert Zierold, Agnes Weimer, Artur Feld, Gerold A. Schneider, Horst Weller, and Andreas Hütten**

The spin-dependent electrical transport in rigid inorganic-inorganic layered systems is extensively applied for the detection of magnetic fields in data storage. In this work, spin-dependent electrical transport in flexible organic-inorganic supercrystals based on superparamagnetic iron oxide nanoparticles is investigated. These nanoparticles are stabilized by oleic acid ligands, which in turn are serving as tunneling barriers between individual magnetic nanoparticles. The resulting tunneling magnetoresistance (TMR) is tunable due to the elastic properties of these organic barriers. Applying external mechanical stress on this composite material will change the average distance between adjacent nanoparticles and will hence determine the resulting TMR-effect amplitude. Thus, measured stress-induced changes in the barrier thickness at sub-nanometer scale allow for determining the mechanical properties of organic barrier molecules in the confined space between the particles. These results provide the foundation for a new type of mechanical sensor.

1. Introduction

The discovery of spin-dependent electrical transport through ferromagnetic/insulator/ferromagnetic layered systems has promoted the design and application of highly sensitive sensors in read heads for data storage. In such devices, the tunneling magnetoresistance (TMR) effect amplitude depends on the relative alignment of the magnetization in adjacent magnetic layers and on the barrier geometry.

Antiparallel alignment of the magnetic moments leads to reduced conductivity (G_M) through the TMR device as a consequence of a hindrance to electron transport based on the presence of a potential barrier φ_M.[1] Under the influence of an increasing external magnetic field and the associated equal alignment of the individual magnetic moments, the potential φ_M decreases steadily. With a complete parallel alignment of the magnetic moments, this potential is finally negligible.

In these TMR devices, typically, an inorganic metal oxide layer with a thickness of 0.5 to 2 nm is chosen as an insulating barrier. Moreover, different organic barriers were studied concerning their electric behavior [2–5], transport mechanism [6–7], and efficiency.[8–9] Especially, oleic acid as one of the most commonly used chemical for surface functionalization of nanoparticles has been investigated as potential barrier material in granular films.[10–14]

In contrast to common TMR devices with an inorganic stiff barrier types the conductivity of the granular organic–inorganic

A. Dreyer, T. Rempel, M. Gottschalk, A. Hütten
Institute of Thin Films and Physics of Nanostructures
Bielefeld University
Universitätsstrasse 25
D-33165 Bielefeld, Germany
E-mail: adreyer@physik.uni-bielefeld.de;
andreas.huetten@uni-bielefeld.de

R. Zierold
Center for Hybrid Nanostructures
Hamburg University
Luruper Chaussee, D-22761 Hamburg, Germany

The ORCID identification number(s) for the author(s) of this article can be found under https://doi.org/10.1002/aelm.202200082.

DOI: 10.1002/aelm.202200082

A. Weimer, A. Feld
The Hamburg Center for Ultrafast Imaging
Hamburg University
Luruper Chausee 149, D-22761 Hamburg, Germany

A. Weimer, A. Feld, H. Weller
Institute of Physical Chemistry
Hamburg University
Grindelallee 117, D-20146 Hamburg, Germany

G. A. Schneider
Institute of Advanced Ceramics
Hamburg University of Technology
Denickestrasse 15, D-21073 Hamburg, Germany

H. Weller
Fraunhofer-CAN
Grindelallee 117, D-20146 Hamburg, Germany

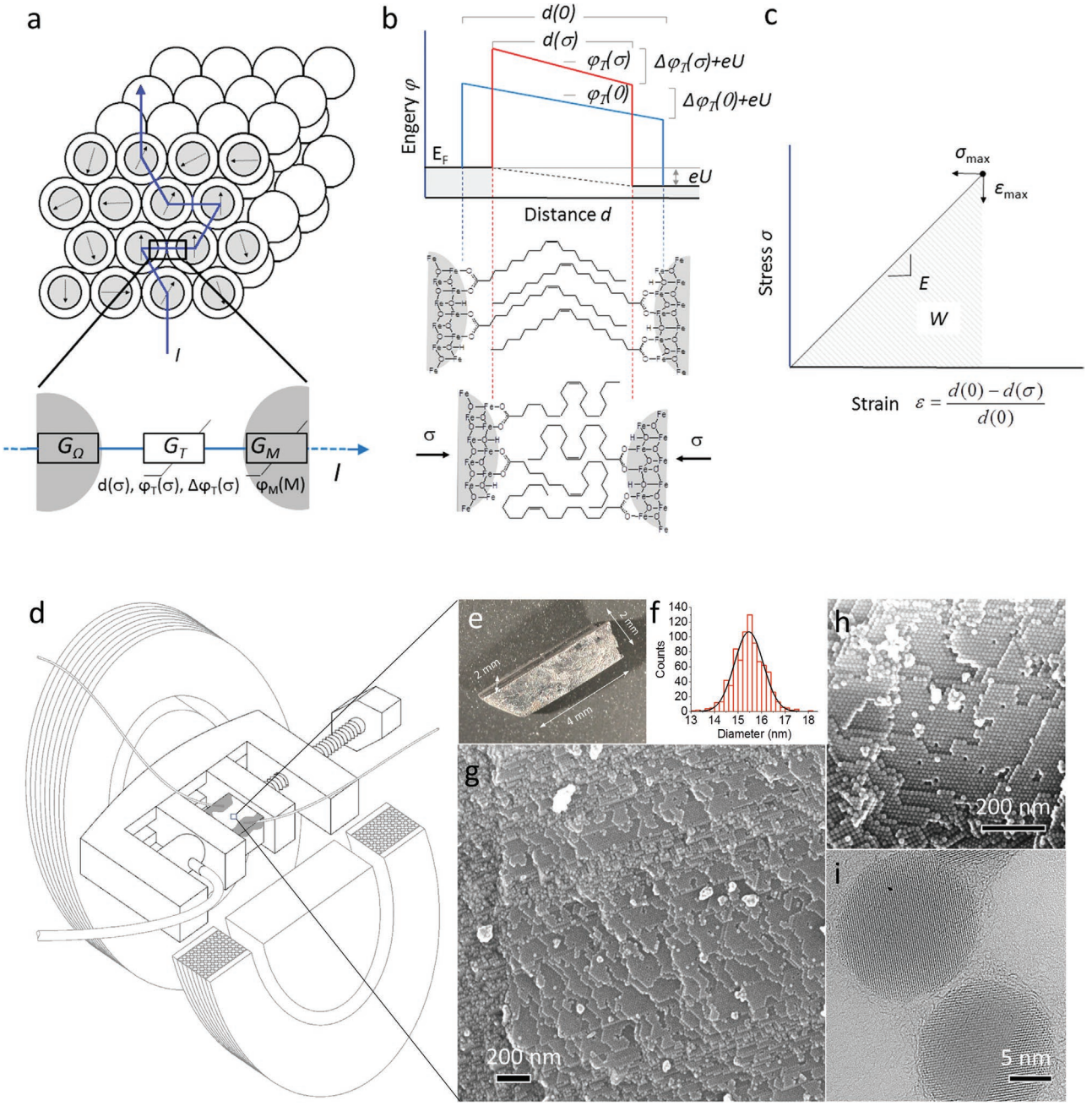

Figure 1. Concept of stress and spin-depending electron transport. a) The current path through the particles (blue) is equivalent to passing through a series of tunnel junctions, where each one consists of three types of conductivities G_{Ω}, $G_{T,}$ and G_{M}. b) According to the Brinkman model, G_T depends strongly on the barrier geometry which is influenced by mechanical stress. c) The stress-depending G_T is transformed into stress-strain diagram illustrating the mechanical behavior of the organic barrier. d) Set-up for the measurement of the stress- and spin-dependent nanocomposite. A plastic clamp with a force sensor fixes the nanocomposite e) in a homogenous magnetic field. f) is the particle size distribution. g) and h) are images of the fractured surface of the nanocomposite obtained by scanning electron microscope (SEM). The high resolution-TEM image of a fine ground nanocomposite i) displays the separation of single particles by oleic acid.

system should not only be influenced by applying an external magnetic field, but also by mechanical stress that controls the average barrier geometry.

However, the influence of acting mechanical forces on the transport properties of a granular system has not been investigated in these films so far.

A combined method of induced self-assembly of stabilized nanoparticles in solution and subsequent pressing of the obtained solid microcrystallites into a compact material allows to organize the organically coated nanoparticles in a periodic structure analogous to a crystal lattice and thus to obtain a centimeter-sized polycrystalline nanocomposite material, shown in simplified form in **Figure 1**a.[15]

A mechanical load can very easily be applied to this nanocomposite and the variable electrical transport properties can be recorded. The structural change induced under mechanical stress in a nanocomposite prepared from oleic acid-stabilized superparamagnetic iron oxide nanoparticles has recently been studied in detail.[16–17] At low mechanical stress, deformation of the soft organic oleic acid layer between the hard inorganic particles first occurs.

The insulating soft layer between the particles thus acts as a force-varying tunnel barrier for electron transport. Figure 1b illustrates the impact of applied mechanical stress on an organic tunnel junction, using the simple geometrical potential. The barrier geometry is described by the barrier height φ_T and asymmetry $\Delta\varphi_T$ and the barrier thickness d. In particular, the thickness of a barrier made of soft organic molecules is influenced by the action of external mechanical forces.

The conductivity G_T resulting from this potential is given by the Brinkman model according to the following Equation (1).[18]

$$G_T = \frac{G_\Omega}{N} \cdot \left[1 - \left(\frac{A_0 \cdot (\Delta\varphi_T)}{16 \cdot (\varphi_T)^{3/2}} \right) \cdot eU + \left(\frac{9 \cdot A_0^2}{128 \cdot (\varphi_T)} \right) \cdot (eU)^2 \right] \quad (1)$$

Here $A_0 = 4e(2m)^{1/2}d/3\hbar$ with d is the barrier thickness, and $\hbar$ is the reduced Planck constant, m is the electron mass, e is the electron charge, and G_Ω is the ohmic ground conductivity of the sample. The additional parameter N takes into account that in the current pathway through the nanocomposite thousands of single tunnel junctions and thus thousands of conductances are interconnected in a serial fashion (Figure 1a).

If mechanical forces and external magnetic fields act simultaneously on the nanocomposite, a single tunnel junction in this nanocomposite can be described electrically by three serial conductivities, as shown in Figure 1a: the constant ohmic particle conductivity G_Ω, the magnetization-dependent conductivity G_M, and the barrier geometry-dependent tunnel conductivity G_T.

For the mathematical description of the easily measurable total conductivity of a nanocomposite under the simulated influence of mechanical forces and magnetic fields, the potential height and asymmetry in the Brinkmann model can be understood as a superposition of two independent single potentials $\varphi_M + \varphi_T$ and their potential asymmetries $\Delta\varphi_M + \Delta\varphi_T$, respectively.

Under the assumption of a variable mechanical force at a constant magnetic field (φ_M and $\Delta\varphi_M$ are constant), the force-dependent barrier properties are accessible by fitting the measured current-voltage characteristics with the modified Brinkman Equation (1).

Thus, the stress-dependent barrier thickness can hence be determined and converted to a classical stress-strain diagram shown in Figure 1c. This approach mediates the mechanical properties of the soft organic molecules in the confined space between the nanoparticles in the nanocomposite.

The described concept allows the first approach to a bifunctional sensor for magnetic fields and mechanical forces, which offers advantages. The mechanical properties of the tunnel barrier can be easily tailored to the sensing application by a suitable choice of organic surface molecules. Due to the isotropic structure of the nanocomposite, forces from different spatial directions can be detected, including shear and torsion. In addition, this sensing material offers a high miniaturization potential.

In this work, we present the first investigations of the force- and magnetization-dependent current-voltage characteristics of a macroscopic inorganic-organic nanocomposite material in which the individual nanoparticles are highly ordered. For this work, we use the well-studied nanocomposite material of monodisperse superparamagnetic iron oxide nanoparticles surrounded by and separated from an oleic acid monolayer.[15–17]

In the following, we will describe the buttom-up synthesis of the nanoparticles, the organization into a well-ordered nanocomposite, and will report on the resulting magnetic properties of the obtained nanocomposite. We present the general physics processes induced by magnetic fields and/or mechanical forces in the nanocomposite. This is done by using the measured current-voltage characteristics of a tunnel barrier around a single particle and the force-dependent current-voltage characteristics of thousands of serial tunnel barriers in the nanocomposite. The Brinkman fitting provides the force-dependent barrier characteristics including the mechanical properties of the olic acid molecules between the particles. In this way, force-induced change trends in barrier thickness can be detected in the sub-nanometer range.

2. Results and Discussion

2.1. Synthesis and Characterization of Nanoparticles

The spherical iron oxide nanoparticles used for the nanocomposite fabrication were synthesized by thermal decomposition of iron(III) oxide-hydroxide in a solution of oleic acid and 1-octadecene at 320 °C.[19] The size and the shape of the particles were controlled by varying the molar ratio of the precursor and the stabilizer and choosing a proper reaction time.[20] Finally, for the nanocomposite fabrication, we used monodisperse particles with a diameter d of (15.5 ± 0.8) nm determined by transmission electron microscopy (TEM), given in Figure 1f. Details of the particle synthesis are given in chapter A of Supporting Information (SI).

These particles are superparamagnetic at room temperature which was proven by vibrating sample magnetometry (VSM) resulting in a blocking temperature of about 210 K. Experimental details of the VSM measurement procedure is given in chapter A of the SI.

Fourier transform infrared spectroscopy proves that each particle core is surrounded by a monolayer of oleic acid molecules bound by their carboxylate groups to the particle surface as it is shown in Figure 1b. By a combination of thermogravimetric analysis and helium pynometry (HeP) the oleic acid coverage was determined to 1.6 molecules per nm^2. Further details concerning the particle characterization are given in chapter A of SI.

2.2. Transport Measurement of a Single Nanoparticle

First, the transport properties of single tunnel junctions were investigated to determine their unaffected barrier geometry. Therefore, larger cubic-shaped particles were synthesized in the same way as the spherical once just by modification of the oleic

acid concentration, the reaction temperature, and the reaction time.[20] More details are given in chapter A of SI. One of these large particles was electrical contacted by positioning it between two conducting paths of a gold double-comb structure on a silicon dioxide substrate. In a dual-beam focused ion beam system, the particle was connected with two thin conducting paths of platinum from gas deposition to each comb structure. The current-voltage characteristics in the range of ± 2 V measured for single particles were fitted by the Brinkman Equation (1) so as to determine the barrier thickness d, height φ_T, and asymmetry $\Delta\varphi_T$.[18]

The obtained mean values for particles with the surrounding oleic acid layer are (0.998 ± 0.079) nm for the barrier thickness, (5.51 ± 0.79) eV for the barrier height, and −(1.04 ± 0.82) eV for the barrier asymmetry. More details are given in chapter B in SI.

2.3. Synthesis and Characterization of the Nanocomposite

The synthesized monodisperse small spherical oleic acid-coated iron oxide particles were arranged to a three-dimensional structure composed of supercrystals following the procedure described in.[15] Stable particle solution was filled into a seal die and particle self-assembly was induced by slow evaporation of the solvent. The obtained sediment was dried and pressed at 150 °C with 260 N mm^{-2} to a solid pellet, which was cut into pieces, compare with Figure 1e.

The resulting nanocomposites were investigated by scanning electron microscopy, high-resolution TEM (HRTEM), and VSM. Nanoparticles of the nanocomposites are ordered in a face-centered cubic superlattice as is shown in Figure 1g,h. Each particle is insulated from adjacent particles by an organic layer, see Figure 1i, with an average thickness d of (0.87 ± 0.56) nm. This average particle distance also ensures that adjacent superparamagnetic nanoparticles do not interact via exchange coupling but still could interact via their magnetic strayfields when magnetized. Isothermal VSM measurements at 300 K indicate that the superparamagnetic behavior of the nanoparticles is preserved after compaction to the macroscopic nanocomposite, as shown in **Figure 2**a,b, implying that the superparamagnetic behavior was not affected by the compaction process.

2.4. Transport Measurement of the Nanocomposite

In the obtained nanocomposite, the oleic acid layers, which are surrounding each iron oxide particle, will serve as tunnel

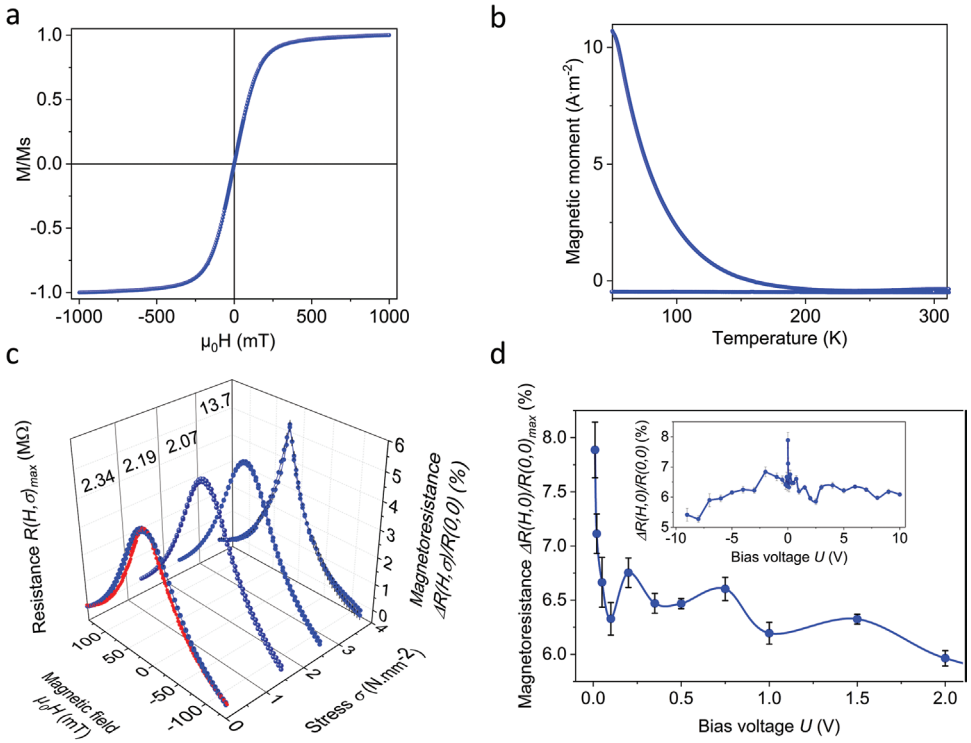

Figure 2. Magnetic and spin-dependent electron transport properties through a nanocomposite. a) The magnetic hysteresis of the nanocomposite at 300 K which clearly shows the superparamagnetic character of the nanocomposite via the zero crossing of the normalized magnetization at a vanishing external magnetic field. b) Alternatively, this superparamagnetic state of the nanocomposite can also be shown by magnetic relaxation measurements. In this case, the nanocomposite is cooled to 50 K, then aligned in the magnetic field of 3 T, and relaxing this state without a field while increasing the temperature. The magnetic remanence disappearing at room temperature is also an indicator of the superparamagnetic behavior of the nanocomposite and thus of the nanoparticles that compose the nanocomposite. c) Representative selection of the measured stress- and magnetic field-depending resistance $\Delta R(H,0)/R(0,0)$ of the nanocomposite. The calculated stress-free magnetoresistive behavior from the measured magnetization is displayed in red. The narrowing of the magnetoresistance responds with increasing strain and hence decreasing distance between the nanoparticles is based on the increasing dipolar interaction between the nanoparticles. This leads to magnetization reversal of whole chains of nanoparticles and is deduced from micromagnetic simulation presented in section E of the Supporting Information. d) The magnetoresistance $\Delta R(H,0)/R(0,0)$ decreases strongly with increasing bias voltage in an oscillating manner shown in the overview (inset) and in detail.

junctions in the transport measurements. Hence, single tunnel junctions are interconnected in a serial and in parallel fashion and support a vast number of possible current pathways. For simplification of the description, a serial interconnected of the single tunnel junctions in the main current pathway through the nanocomposite can be assumed.

To measure the transport properties, pieces of the nanocomposite were polished and electrically contacted with two copper wires by silver soldering at a distance of 1 mm, which corresponds to approximately 60×10^3 to 64×10^3 serial tunnel junctions. The sample was fixed in a plastic screw clamp together with a force sensor and all was positioned in an adjustable homogenous magnetic field generated by two magnetic coils. The measurement setup is schematically shown in Figure 1d. All measurements were performed at constant room temperature to exclude thermal influences.[21] The current I through the nanocomposite at an applied voltage U was measured, thus the resistance R was recorded depending on an external magnetic field H and applied mechanical stress σ. More details are given in chapter C of SI.

2.4.1. Magnetic Field-Depending Transport (G_M)

Measured resistance $R(H,\sigma)$ of the nanocomposite with a bias voltage U of 1 V is depicted in Figure 2c. The resistance $R(0,0)$ is in the order of 2.3 MΩ. An increasing magnetic field $\mu_0 H$ from 0 to 136 mT parallel to the current flow aligns the single-particle moments successively and changes the resulting TMR-effect amplitude $\Delta R(H,0)/R(0,0)$ between 4% and 8% for different samples pieces. The magnetic saturation of each sample was not achieved in these measurements as expected from the magnetization measurements. These TMR amplitudes are in accord with published values for small nanoparticle ensembles.[9,13–14]

Based on the superparamagnetic behavior of the nanocomposite, the magnetoresistance is not hysteretic. The measured TMR characteristics can be described as a sequential spin-dependent tunneling phenomenon in a granular system using $\frac{\Delta R(H,0)}{R(0,0)} = \frac{M^2 \cdot P^2}{1 + M^2 \cdot P^2}$.[22] Here, M is the normalized magnetization from Figure 2a and P is the spin polarization of 0.29 for the iron oxide hematite.[23] In this way calculated TMR behavior for a stress-free nanocomposite is displayed in Figure 2c as a red curve.

The magnetoresistance is strongly influenced by the bias voltage U as can be seen in Figure 2d. For increasing bias voltages U from 10 mV to 10 V, the magnetoresistance drops in an oscillating curve characteristic by 22%. The oscillation frequency was observed for different samples.

An oscillating behavior was already experimentally observed for cobalt particles with diameters about $d = 2.5$ nm embedded in an aluminum oxide matrix located in a nanosized gap between two point-shaped electrodes at 4.5 K.[24] The oscillation in this paper is explained with a Coulomb blockade in the current pathway caused by different charging and discharging states of the Co particles and with the opening of additional pathways at higher bias voltages.[25] Electrons accumulate at particles with the highest resistance in each current pathway. Opening up additional electron tunneling pathways, the electrostatic repulsion energy of the charged particle had to overcome by the applied bias voltage or the thermal energy.

We assume that a Coulomb blockade is also rising for the detected oscillation in the magnetoresistance versus bias voltages curves of our nanocomposite. That the oscillation is still observable at room temperature indicates a high electrostatic repulsion due to high particle charging.[26] This charging can be explained by the coordinating binding of the negative carboxylate group of the oleic acid to the particle surface leading to a measurable zeta potential of the particle in the water of –476 mV which is close to the observable bias voltage period given in Figure 2d. This oscillation period increasingly blurred after applying a voltage to the nanocomposite of around 10 V because of the decomposition of the oleic acid molecules at this condition apparent in the inset of Figure 2d. Please refer to further details in chapter D of SI, where the resulting Coulomb blockages are calculated.

2.4.2. Stress-Depending Transport (G_T)

Not only the externally applied magnetic field influences the transport behavior, but mechanical stress on the soft organic barrier effects the transport, too. Following the classical resistance picture, applying mechanical compressive stress to the nanocomposites shifts their electric resistance to smaller values, but quantum mechanically to larger transmission and hence larger TMR-effect amplitudes. Simultaneously, narrowing the distance between adjacent nanoparticles will increase their strayfield interactions resulting in a collective magnetic switching of domains of many nanoparticles, which is indicated by narrower magnetoresistance characteristics and decreasing TMR-effect-amplitudes, see in Figure 2c. Details concerning the micromagnetic simulation can be found in Chapter E of SI.

The magnetic field-free resistance $R(0,\sigma)$ decreases continuously with rising applied compressive stress to the nanocomposite shown in **Figure 3**a. After each loading, the sample was allowed to relax again to distinguish an elastic and an inelastic part of resistance changes. The inelastic fraction of the total resistance change is (29.3 ± 2.4)%.

Under loading stress above 2.5 N mm^{-2}, the resistance increases suddenly to much higher values than the initial resistance. A macroscopic material failure is not observable at this state which takes place only at higher loading stresses of about 50 N mm^{-2}.

We obtain more details on the stress-induced changes inside the organic barrier from stress-depending current-voltage characteristics shown in Figure 3b. From this data, Equation (1) gives access to the thickness d, height φ and asymmetry $\Delta\varphi$ of the barrier depending on the applied mechanical stress σ.

It should be noted that the total current through the nanocomposite is determined by the serial ohmic (G_Ω), spin-dependent (G_M), and the spin-independent (G_T) conductivities of each tunnel junction in the current pathway as is pictured in Figure 1a. However, Equation (1) describes only the part of the total current that is caused by the spin-independent conductivity G_T. This fraction must be separated. Hence, the linear and stress-independent G_Ω was extracted from the measured

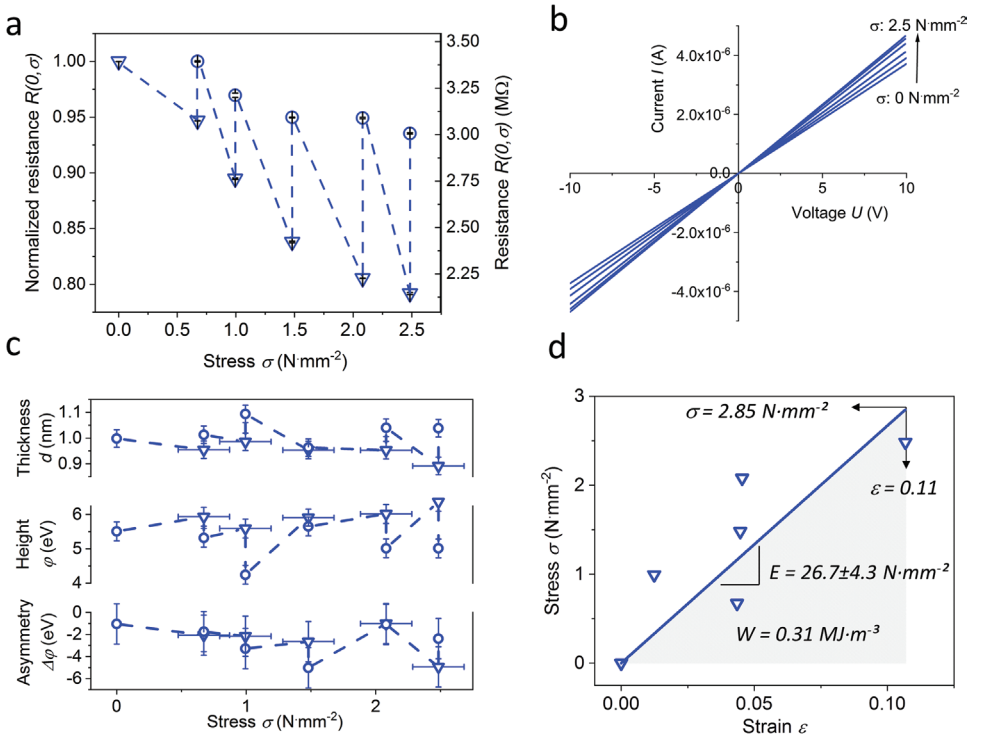

Figure 3. Mechanical barrier properties a) The field-free resistance R(0,σ) of the nanocomposite decreases with applied mechanical stress (triangle). After each loading the sample was relaxed again (circles). b) Current voltage characteristic of nanocomposite for different applied mechanical stress σ applying a step width 0.5 N mm^{-2}. From these curves, the barrier parameters were calculated by the modified Brinkman equation (1) as functions of the applied mechanical stress and are presented in c). As can be seen there are six pairs of data. d) These six obtained barrier thicknesses $d(\sigma)$ are converted into stress-dependent strain. Based on the observed relaxation in (c), the stress-strain values are adjusted by a linear fit considering Hook's law, resulting in the elastic modulus E, the ultimate stress σ, the tensile strain ε, and the energy absorption capacity W of the organic barriers.

current-voltage characteristic. G_M and G_T can be described as contributions to the barrier height ($\varphi_M + \varphi_T$) and asymmetry ($\Delta\varphi_M + \Delta\varphi_T$). The spin-dependent contributions φ_M and $\Delta\varphi_M$ were determined by fitting the stress-free current-voltage characteristic by Equation (1) with the barrier parameters obtained from the single barrier measurements as described above. For the stress-dependent current-voltage characteristic fits, φ_M and $\Delta\varphi_M$ were set as constant. This assumption is reasonable when comparing the stress-independent behavior of the magnetoresistance $\Delta R(H,0)/R(0,0)$, as can be seen in Figure 2c. Hereby, the stress-dependent barrier geometry is obtained and shown in Figure 3c. The errors given are mean standard deviations from three independent measurements. Details on the fitting procedure is given in chapter F in SI.

As expected, the barrier thickness $d(\sigma)$ drops under load and expands after relaxation. This result is converse to the observed behavior of the barrier height $\varphi(\sigma)$. The molecular orbitals of the oleic acid molecules overlap under load. According to the Pauli exclusion principle, electrons have to avoid into high-energy orbitals with the consequence that the barrier height increases as observed.

In Figure 3d, the stress-dependent barrier thickness is converted into a strain by $\varepsilon = \frac{d(0) - d(\sigma)}{d(0)}$. The obtained stress-strain curve provides convincing mechanical properties of the organic barrier molecules in confined space between the hard nanoparticles. The slope represents the elastic moduli of the organic layer coating the nanoparticles. Figure 3c shows the result with a resulting elastic modulus E of (26.7 ± 4.3) N mm^{-2} and an abrupt nanoscopic material failure at a strength of 2.5 N mm^{-2}. For the compression of a Langmuir-Blodgett film of the same particles on a water surface, we found a comparable elastic modulus of (13.7 ± 3.1) N mm^{-2}. Details concerning these experiments can be found in chapter G in SI.

The integral of the stress-strain curve represents the energy absorption capability W of our nanocomposite until material failure at 0.16 MJ m^{-3}. The material failure starts and takes place in the soft organic phase of the nanocomposite.[15–17] Therefore, the energy absorption value is that of the organic barrier molecules.

3. Conclusion

A soft organic barrier in a superparamagnetic nano-granular tunnel device allows the detection of external magnetic fields by the change in their magnetization as well as the detection of mechanical stress by changes in their average barrier geometry. The barrier thickness changes under a moderate mechanical load at the sub-nanometer scale. Consequently, measured stress-induced changes in the barrier thickness at the sub-nanometer scale allow for determining the mechanical properties of organic barrier molecules in the confined space between the particles. This provides the foundation of a new type of mechanical sensor.

Supporting Information

Supporting Information is available from the Wiley Online Library or from the author.

Acknowledgements

The authors acknowledge financial support from the German Research Foundation (DFG) via 192346071-SFB 986 projects A1, A6, and C5. Also, we wish to thank Bielefeld University and their faculty of Physics for support with experiments and analytics.

Open access funding enabled and organized by Projekt DEAL.

Conflict of Interest

The authors declare no conflict of interest.

Author Contributions

A.D. fabricated the nanocomposite, initiated the investigation of the stress- and spindepending transport, and chose the required analytical methods. A.H. enables these studies by the experimental set-up and supports the interpretation of the results with simulations. A.F. and A.W. synthesized and analyzed the nanoparticles supervised by H.W. The fabrication of the nanocomposite was supervised by G.A.S. The magnetic characterization of a single particle and a particle ensemble was done by M.G. and R.Z., respectively. T.R. performed the TMR measurement.

Data Availability Statement

The data that support the findings of this study are available from the corresponding author upon reasonable request.

Keywords

force sensor, nanoparticle, organic barrier, supercrystal, tunneling conductance

Received: January 21, 2022
Revised: April 8, 2022
Published online: May 26, 2022

[1] M. Jullière, *Phys. Lett. A* **1975**, *54*, 225.
[2] C. Herrmann, G. C. Solomon, M. A. Ratner, *J. Chem. Phys.* **2011**, *134*, 224306.
[3] V. A. Dediu, L. E. Hueso, I. Bergenti, C. Taliani, *Nature Mater.* **2009**, *8*, 707.
[4] Z. H. Xiong, D. Wu, Z. V. Vardeny, J. Shi, *Nature* **2004**, *427*, 821.
[5] F. Fabris, E. LimaJr, C. Quinteros, L. Neñer, M. Granada, M. Sirena, R. D. Zysler, H. E. Troiani, V. Leborán, F. Rivadulla, E. L. Winkler, *Phys. Rev. Appl.* **2019**, *11*, 054089.
[6] C. Barraud, P. Seneori, R. Mattana, S. Fusil, K. Bouzehouane, C. Deranlot, P. Graziosi, L. Hueso, I. Bergenti, V. Dediu, F. Petroffi, A. Fert, *Nat. Phys.* **2010**, *6*, 615.
[7] S. Usmani, M. Lepesant, A. Bupathy, T. Blon, L.-M. Lacroix, V. Banerjee, B. Chaudret, J. Carrey, *Phys. Rev. B* **2018**, *98*, 104433.
[8] T. S. Santos, J. S. Lee, P. Migdal, I. C. Lekshmi, B. Satpati, J. S. Moodera, *Phys. Rev. Lett.* **2007**, *98*, 016601.
[9] A. Mitra, B. Barick, J. Mohapatra, H. Sharma, S. S. Meena, M. Aslam, *AIP Adv.* **2016**, *6*, 055007.
[10] L. Xi, J. H. Du, J. H. Ma, Z. Wang, Y. L. Zuo, D. S. Xue, *J. Alloys Compd.* **2013**, *550*, 365.
[11] H. E. Romero, M. Drndic, *Phys. Rev. Lett.* **2005**, *95*, 156801.
[12] C. T. Black, C. B. Murray, R. L. Sandstorm, S. Sun, *Science* **2000**, *290*, 1131.
[13] S. Bedanta, W. Kleemann, *J. Phys. D: Appl. Phys.* **2009**, *42*, 013001.
[14] H. Zeng, C. T. Black, R. I. Sandstrom, P. M. Rice, C. B. Murray, S. Sun, *Phys. Rev. B* **2006**, *73*, 020402.
[15] A. Dreyer, A. Feld, A. Kornowski, E. D. Yilmaz, H. Noei, A. Meyer, T. Krekeler, C. Jiao, A. Stierle, V. Abetz, H. Weller, G. A. Schneider, *Nat. Mater.* **2016**, *15*, 522.
[16] D. Giuntini, S. Zhao, T. Krekeler, M. Li, M. Blankenburg, B. Bor, G. Schaan, B. Domènech, M. Müller, I. Scheider, M. Ritter, G. A. Schneider, *Sci. Adv.* **2021**, *7*.
[17] D. Giuntini, A. Davydok, M. Blankenburg, B. Domènech, B. Bor, M. Li, I. Scheider, C. Krywka, M. Müller, G. A. Schneider, *Nano Lett.* **2021**, *21*, 2891.
[18] W. F. Brinkman, R. C. Dynes, J. M. Rowell, *J. Appl. Phys.* **1970**, *41*, 1915.
[19] W. W. Yu, J. C. Falkner, C. T. Yavuz, V. L. Colvin, *Chem. Commun.* **2004**, *20*, 2306.
[20] A. Feld, A. Weimer, A. Kornowski, N. Winckelmans, J.-P. Merkl, H. Kloust, R. Zierold, C. Schmidtke, T. Schotten, M. Reidner, S. Bals, H. Weller, *ACS Nano* **2019**, *13*, 152.
[21] A. Useinov, H.-H. Lin, C.-H. Lai, *Sci. Rep.* **2017**, *7*, 8357.
[22] J. Inoue, S. Maekawa, *Phys. Rev. B* **1996**, *53*, *18*, 11927.
[23] M. Catti, G. Valerio, R. Dovesi, *Phys. Rev. B* **1995**, *51*, 7441.
[24] K. Yakushiji, S. Mitani, K. Takanashi, S. Takahashi, S. Maekawa, H. Imamura, H. Fujimori, *Appl. Phys. Lett.* **2001**, *78*, 515.
[25] J. Barnás, A. Fert, *Phys. Rev. Lett.* **1998**, *80*, 1058.
[26] V. Ray, R. Subramanian, P. Bhadrachalam, L.-C. Ma, C.-U. Kim, S. J. Koh, *Nat. Nanotechnol.* **2008**, *3*, 603.